Different ways to evaluate graviton mass

А.Ф. Захаров (Alexander F. Zakharov)

- **E-mail: zakharov@itep.ru**
-
- ***Institute of Theoretical and Experimental Physics,***
- ***B. Cheremushkinskaya, 25, 117218 Moscow***

- ***Bogoliubov Laboratory of Theoretical Physics***
- ***Joint Institute for Nuclear Research, Dubna, Russia***
-

XXXI International workshop on high energy physics "Critical points in the modern particle physics“

Institute for High Energy Physics, Protvino, Russia

07.07.2017

- Co-authors: P. Jovanovic, D. Borka, V. Borka Jovanovic

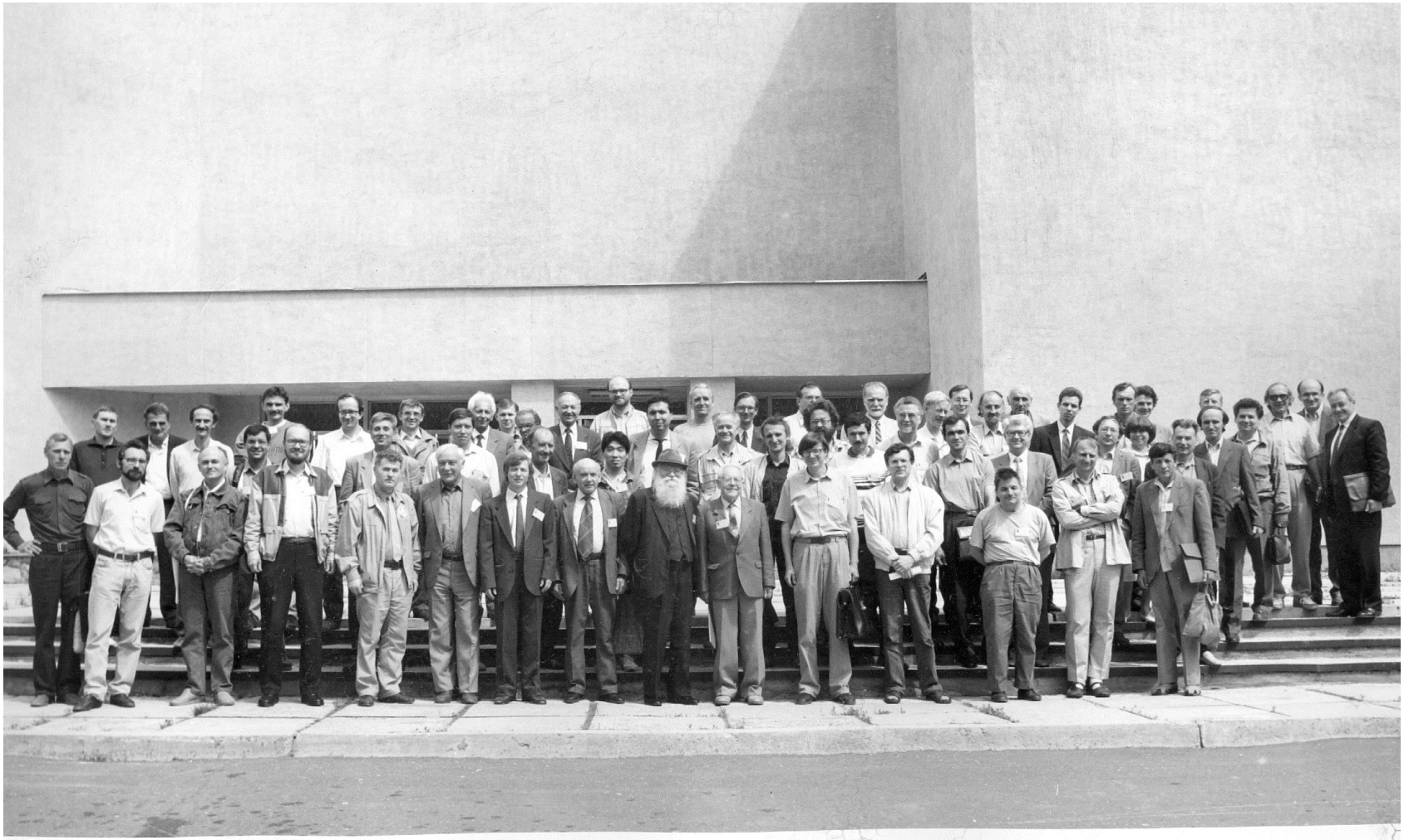

Международный семинар посвященный 140-летию со дня рождения Анри Пуанкаре
Протвино, 27 июня — 1 июля 1994г.

Outline of my talk

- Trajectories of bright stars near the GC as a tool to evaluate a gravitational potential (Kepler – Hooke – Newton – Rutherford potential reconstruction for the GC)
- Massive graviton theories
- Graviton mass evaluation for GW signal
- Graviton mass evaluation from S2 star trajectories
- Conclusions

References

- D. Borka, P. Jovanovic, V. Borka Jovanovic and AFZ, Physical Reviews D, **85**, 124004 (2012).
- D. Borka, P. Jovanovic, V. Borka Jovanovic and AFZ, Journal of Cosmology and Astroparticle Physics, **11**, 050 (2013).
- AFZ, Physical Reviews D **90**, 062007 (2014).
- AFZ, D. Borka, P. Jovanovic, V. Borka Jovanovic, Advances in Space Research 54, 1108 (2014).
- AFZ, J Astrophys. Astron. **36**, 539 (2015)
- AFZ , P. Jovanovic, D. Borka, V. Borka Jovanovic, gr-qc: 1605.00913v; JCAP (2016)
- AFZ, P.Jovanovic, D. Borka, and V. Borka Jovanovic, EPJ Web of Conferences 125, 01011 (2016).

F. Dyson expressed a skepticism in paper "Is a graviton detectable?" (International Journal of Modern Physics A Vol. 28, No. 25 (2013) 1330041 (14 pages))

In spite of difficulties to detect a graviton there are different ways to evaluate its mass

(A. S. Goldhaber, M. M. Nieto, 2010; C. DeRham et al. 2017)

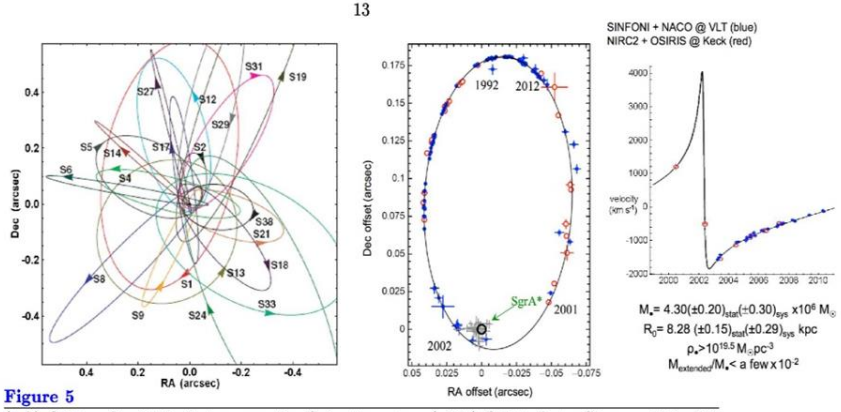

Figure 5

(*left*) Orbits of individual stars near the Galactic center. (*right*) Orbit of star S2 around the BH and associated radio source Sgr A* based on observations of its position from 1992 to 2012. Results from the Ghez group using the Keck telescope and from the Genzel group using the Europen Very Large Telescope (VLT) are combined. This figure is updated from Genzel, Eisenhauer & Gillessen (2010) and is kindly provided by Reinhard Genzel.

These results establish the existence and mass of the central dark object beyond any reasonable doubt. They also eliminate astrophysical plausible alternatives to a BH. These include brown dwarfs and stellar remnants (e. g., Maoz 1995, 1998; Genzel et al. 1997, 2000; Ghez et al. 1998, 2005) and even fermion balls (Ghez et al. 2005; GEG10). Boson balls (Torres et al. 2000; Schunck & Mielke 2003; Liebling & Palenzuela 2012) are harder to exclude; they are highly relativistic, they do not have hard surfaces, and they are consistent with dynamical mass and size constraints. But a boson ball is like the proverbial elephant in a tree: it is OK where it is, but how did it ever get there? GEG10 argue that boson balls are inconsistent with astrophysical constraints based on AGN radiation. Also, the Soltan (1982) argument implies that at least most of the central dark mass observed in galaxies grew by accretion in AGN phases, and this quickly makes highly relativistic objects collapse into BHs. Finally (Fabian 2013), X-ray AGN observations imply that we see, in some objects, material interior to the innermost stable circular orbit of a non-rotating BH; this implies that these BHs are rotating rapidly and excludes boson balls as alternatives to all central dark objects. Arguments against the most plausible BH alternatives – failed stars and dead stars – are also made for other galaxies in Maoz (1995, 1998) and in Bender et al. (2005). Exotica such as sterile neutrinos or dark matter WIMPs could still have detectable (small) effects, but we conclude that they no longer threaten the conclusion that we are detecting supermassive black holes.

KR95 was titled "Inward Bound – The Search for Supermassive Black Holes in Galactic Nuclei." HST has taken us essentially one order of magnitude inward in radius. A few other telescopes take us closer. But mostly, we are still working at 10^4 to 10^5 Schwarzschild radii. In our Galaxy, we have observed individual stars in to $\sim$ 500 Schwarzschild radii. Only the velocity profiles of relativistically broadened Fe Kα lines (e. g., Tanaka et al. 1995; Fabian 2013) probe radii that are comparable to the Schwarzschild radius. So we are still inward bound. Joining up our measurements made at thousands of r_S with those probed by Fe Kα emission requires that we robustly integrate into our story the rich and complicated details of AGN physics; that is, the narrow– and broad–emission-line regions. That journey still has far to go.

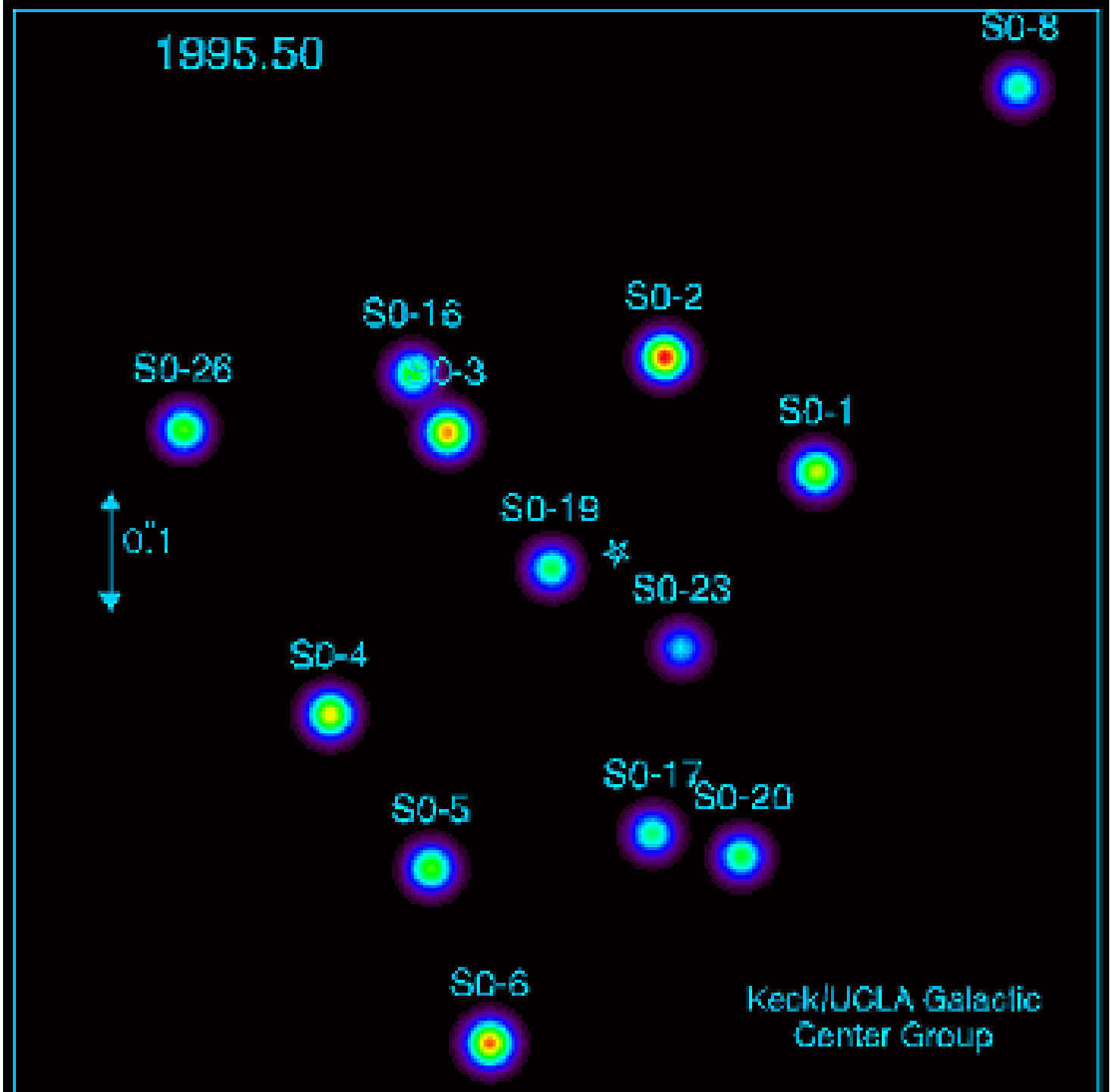
1995.50
S0-8
S0-16
S0-2
S0-26
S0-3
S0-1
0.1
S0-19
S0-23
S0-4
S0-17
S0-20
S0-5
S0-6
Keck/UCLA Galactic
Center Group

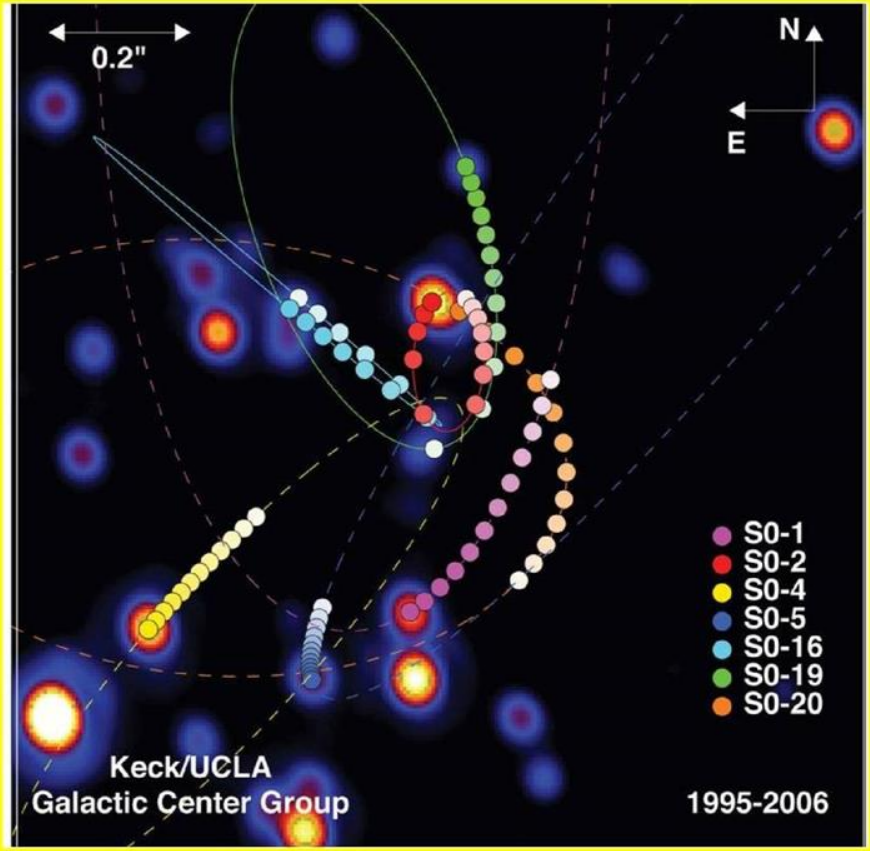

Figure 19: Bright stars near the Galactic Centre.

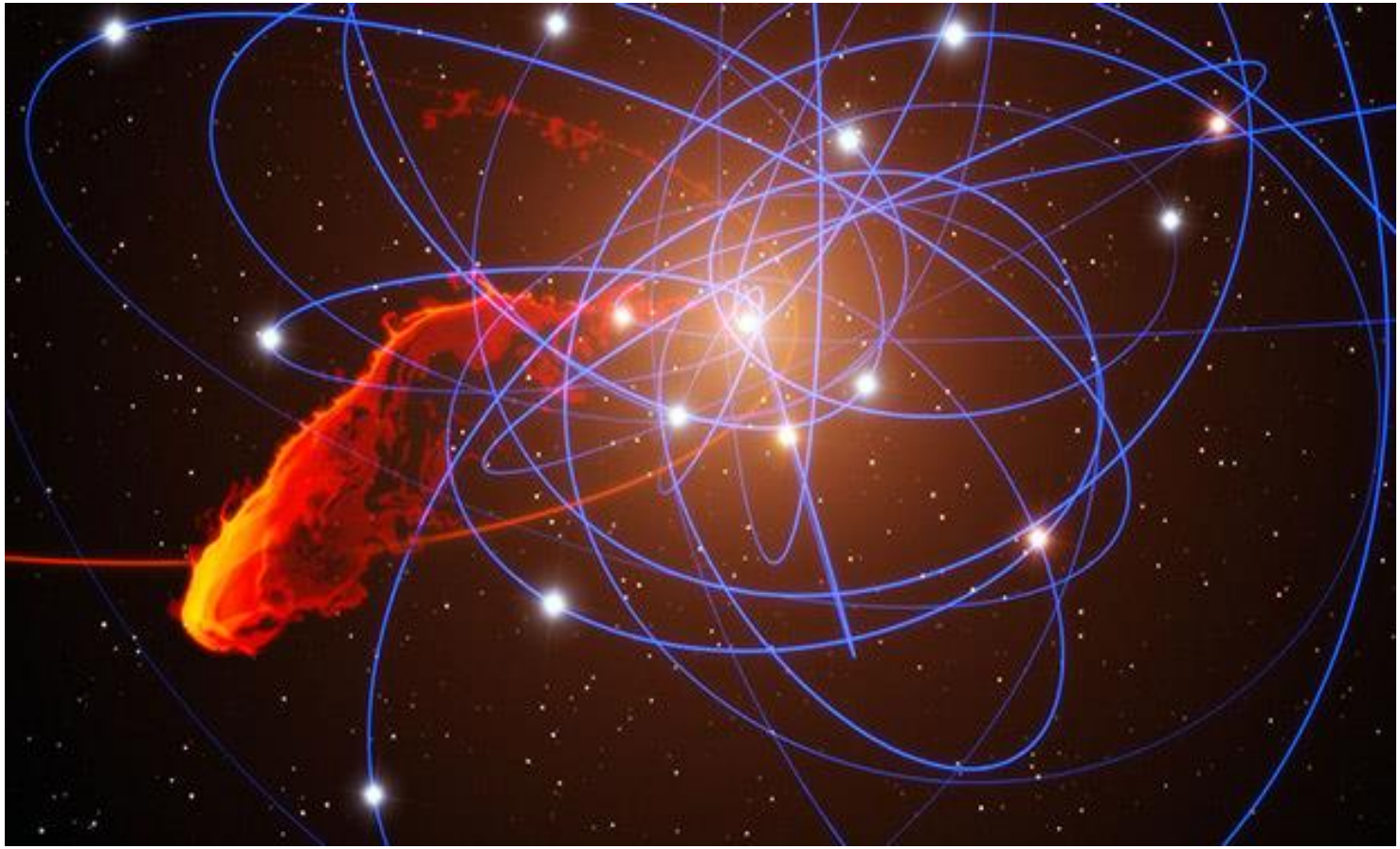

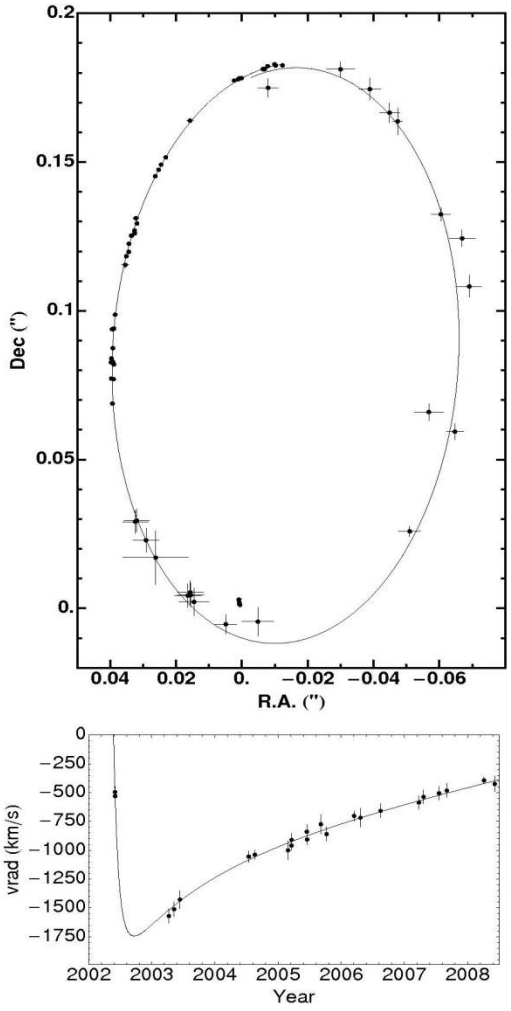

FIG. 13.— Top: The S2 orbital data plotted in the combined coordinate system and fitted with a Keplerian model in which the velocity of the central point mass and its position were free fit parameters. The non-zero velocity of the central point mass is the reason why the orbit figure does not close exactly in the overlap region 1992/2008 close to apocenter. The fitted position of the central point mass is indicated by the elongated dot inside the orbit near the origin; its shape is determined from the uncertainty in the position and the fitted velocity, which leads to the elongation. Bottom: The measured radial velocities of S2 and the radial velocity as calculated from the orbit fit.

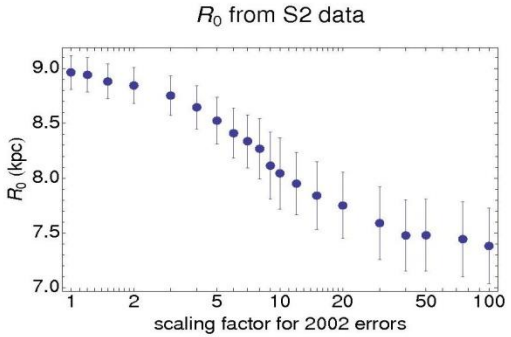

FIG. 14.— Fitted value of R_0 for various scaling factors of the S2 2002 data, using a fit with the coordinate system priors. The factor by which the 2002 astrometric errors of the S2 data is scaled up strongly influences the distance. The mean factor determined in Figure 9 is ≈ 7, corresponding to $R_0 \approx 8.1$kpc.

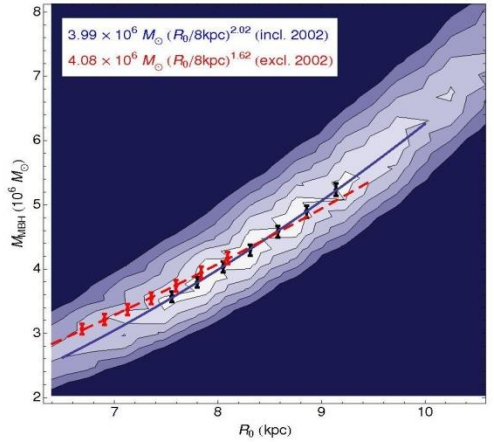

FIG. 15.— Contour plot of χ^2 as function of R_0 and central point mass. The two parameters are strongly correlated. The contours are generated from the S2 data including the 2002 data; fitting at each point all other parameters both of the potential and the orbital elements. The black dots indicate the position and errors of the best fit values of the mass for the respective distance; the blue line is a power law fit to these points; the corresponding function is given in the upper row of the text box. The central point is chosen at the best fitting distance. The red points and the red dashed line are the respective data and fit for the S2 data excluding the 2002 data; the fit is reported in the lower row of the text box. The contour levels are drawn at confidence levels corresponding to 1σ, 3σ, 5σ, 7σ, 9σ.

From the numbers it seems that the fit excluding the

An Expanded View of the Universe

Science with the European Extremely Large Telescope

Black Holes

Black holes are some of the most bizarre objects in the Universe, challenging the imaginations of even the most creative scientists. They are places where gravity trumps all other forces in the Universe, pushing our understanding of physics to the limit. Even more strangely, supermassive black holes seem to play a key role in the formation of galaxies and structures in the Universe.

Galactic Centre

Over the last 15 years or so, an enormous amount of work has gone into improving our understanding of the closest supermassive black hole — Sagittarius A* at the centre of the Milky Way.

Technological progress, in particular in the areas of adaptive optics and high angular resolution with ground-based 8-metre-class telescopes, has allowed impressive progress in understanding supermassive black holes and their surroundings. Key progress was made in proving the very existence of a supermassive black hole at the centre of the Milky Way, in refining our knowledge of how matter falls into black holes, and in identifying gas discs and young stars in the immediate vicinity of the black hole. The Galactic Centre was thus established as the most important laboratory for the study of supermassive black holes and their surroundings.

But its potential for progress in fundamental physics and astrophysics is far from being fully exploited. The Galactic Centre remains the best place to test general relativity directly in a strong gravitational field. The E-ELT will enable extremely accurate measurements of the positions of stars (at the 50–100 microarcsecond level over fields of tens of arcseconds), as well as radial velocity measurements with about 1 km/s precision, pushing our observations ever closer to the black hole event horizon. Stars can then be discovered at 100 Schwarzschild radii, where orbital velocities approach a tenth of the speed of light. This is more than ten times closer than can be achieved with the current generation of telescopes. Such stellar probes will allow us to test the predicted relativistic signals of black hole spin and the gravitational redshift caused by the black hole, and even to detect gravitational wave effects. Further out, the dark matter distribution around the black hole, predicted by cold dark matter cosmologies (ΛCDM), can be explored. The distance to the Galactic Centre can be measured to 0.1%, constraining in turn the size and shape of the galactic halo and the Galaxy's local rotation speed to unprecedented levels. Crucial progress in our understanding of the interaction of the black hole with its surroundings will be made. The puzzling stellar cusp around the Galactic Centre, as well as the observed star formation in the vicinity of the black hole will be studied in detail for the first time.

Left: Very Large Telescope (VLT) observations have revealed that the supermassive black hole closest to us is located in the centre of the Milky Way.

The Milky Way's central supermassive black hole has been weighed by measuring the proper motions of stars in its vicinity.

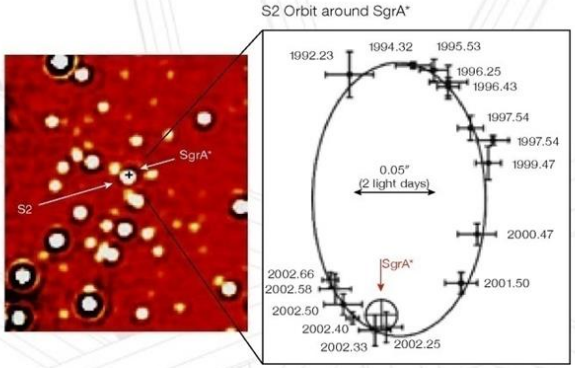

The VLT, *Very Large Telescope*
4 european 8 m telescopes at Cerro Paranal in Chili

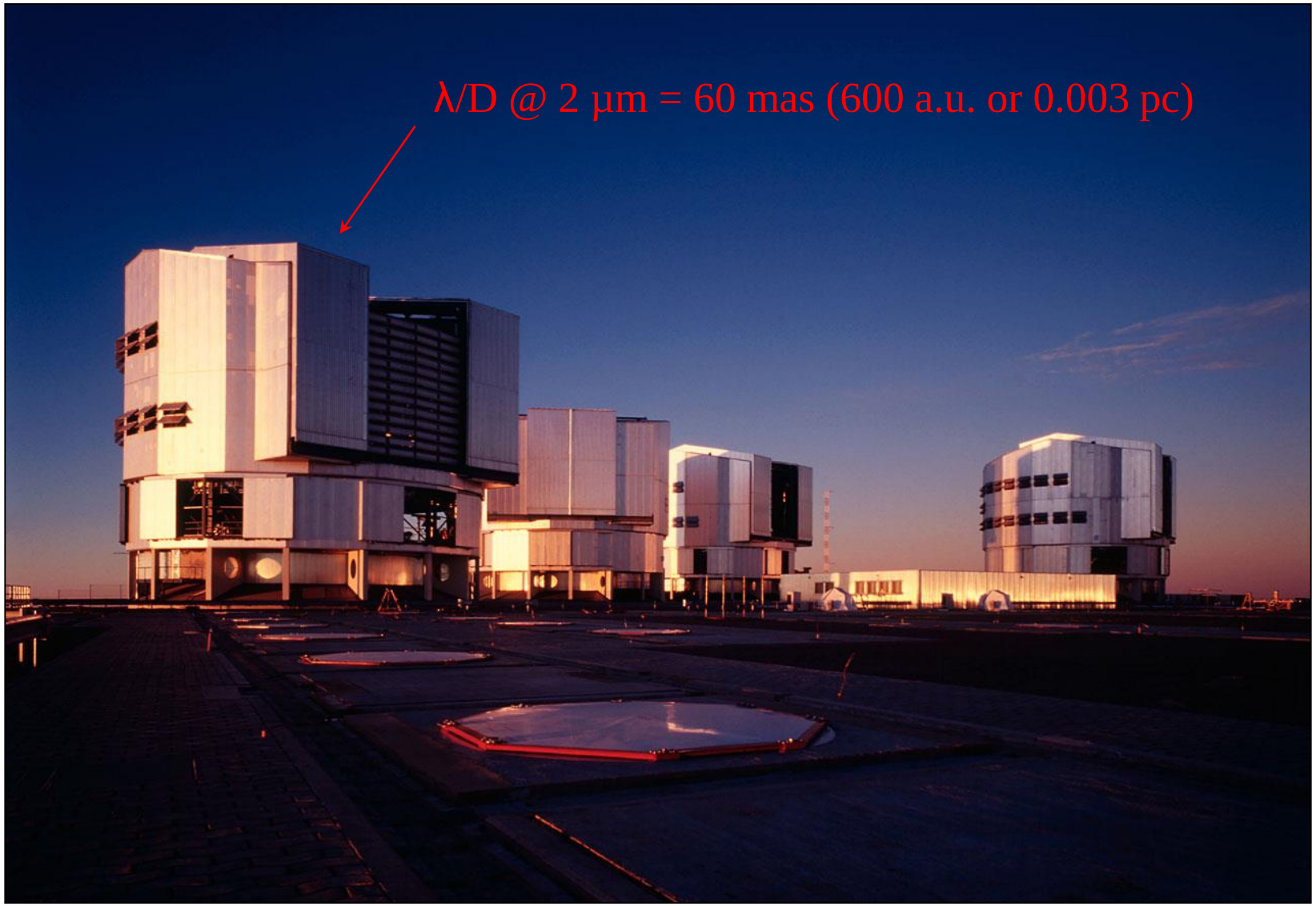

Going beyond boundaries thanks to accurate spatial information

- Bring the ultimate evidence that Sgr A* is a black hole: the mass is contained in the Schwarzschild radius.
- Understand the nature of flares.
- Use the black hole as a tool to study general relativity in the strong field regime

Scale ~ 1 R_s 10 µas

- Study relativistic effects on nearby stars
- Understand the nature of S stars and their distribution

Scale ~ 100 R_s 1 mas

AFZ, A.A. Nucita, F. De Paolis, G. Ingrosso, PRD 76, 062001 (2007)

The mass concentration at the Galactic Center

Recent advancements in infrared astronomy are allowing to test the scale of the mass profile at the center of our galaxy down to tens of AU. With the Keck 10 m telescope, the proper motion of several stars orbiting the Galactic Center black hole have been monitored and almost entire orbits, as for example that of the S2 star, have been measured allowing an unprecedent description of the Galactic Center region. Measurements of the amount of mass $M(< r)$ contained within a distance r from the Galactic Center are continuously improved as more precise data are collected. Recent observations (Ghez et al. (2003)) extend down to the periastron distance ($\simeq 3 \times 10^{-4}$ pc) of the S16 star and they correspond to a value of the enclosed mass within $\simeq 3 \times 10^{-4}$ pc of $\simeq 3.67 \times 10^{6}$ $M_{\odot}$. Several authors have used these observations to model the Galactic Center mass concentration. Here and in the following, we use the three component

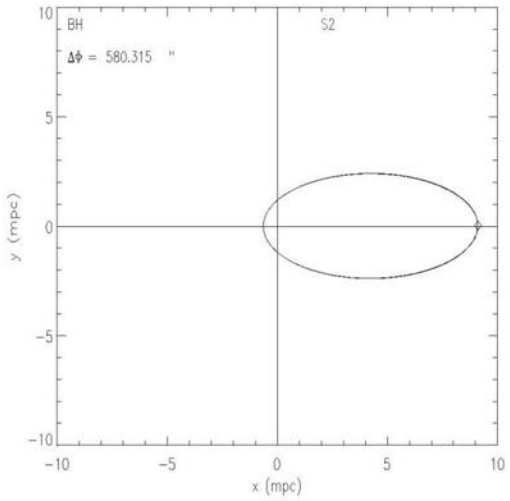
BH
S2
Δφ = 580.315 "
y (mpc)
x (mpc)

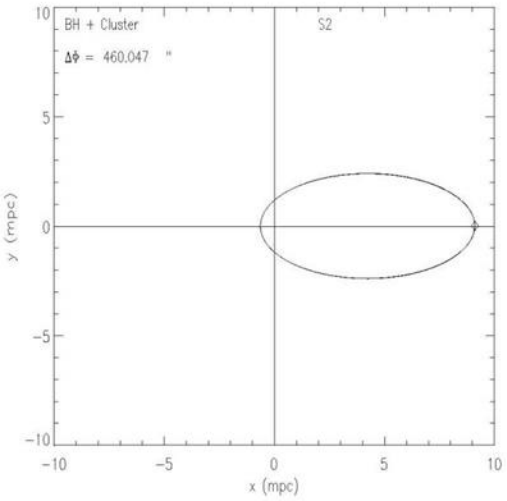
BH + Cluster
S2
Δφ = 460.047 "
y (mpc)
x (mpc)

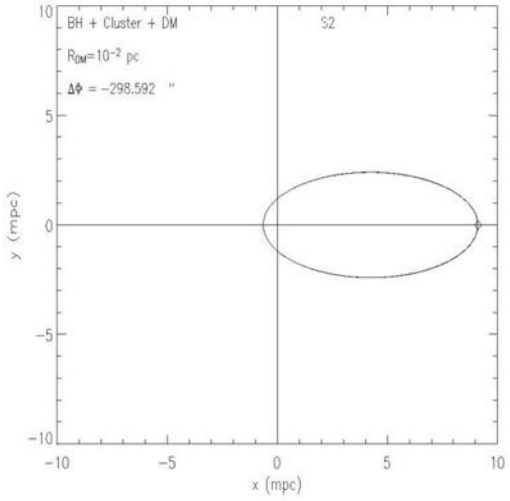
BH + Cluster + DM
S2
R_DM=10^-2 pc
Δφ = -298.592 "
y (mpc)
x (mpc)

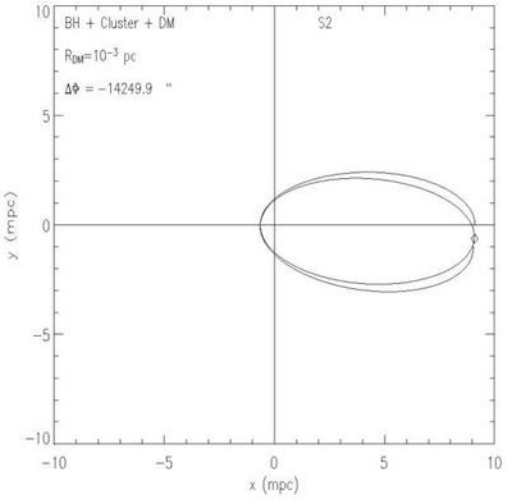
BH + Cluster + DM
S2
R_DM=10^-3 pc
Δφ = -14249.9 "
y (mpc)
x (mpc)

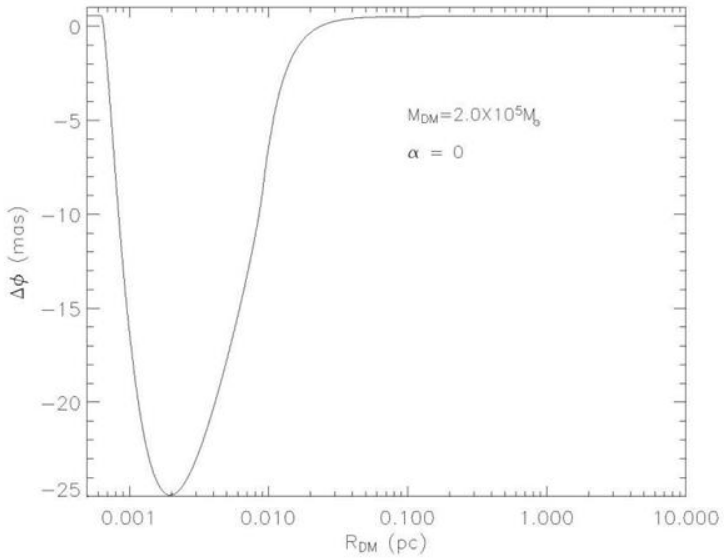

Figure 32: Apoastron shift as a function of the DM radius R_{DM} for $\alpha = 0$ and $M_{DM} \simeq 2 \times 10^5$ M$_\odot$. Taking into account present day precision for the apoastron shift measurements (about 10 mas) one can say that DM radii R_{DM} in the range $8 \times 10^{-4} - 10^{-2}$ pc are not acceptable.

D. Borka, P. Jovanovic, V. Borka Jovanovic and AFZ, PRD, **85**, 124004 (2012).

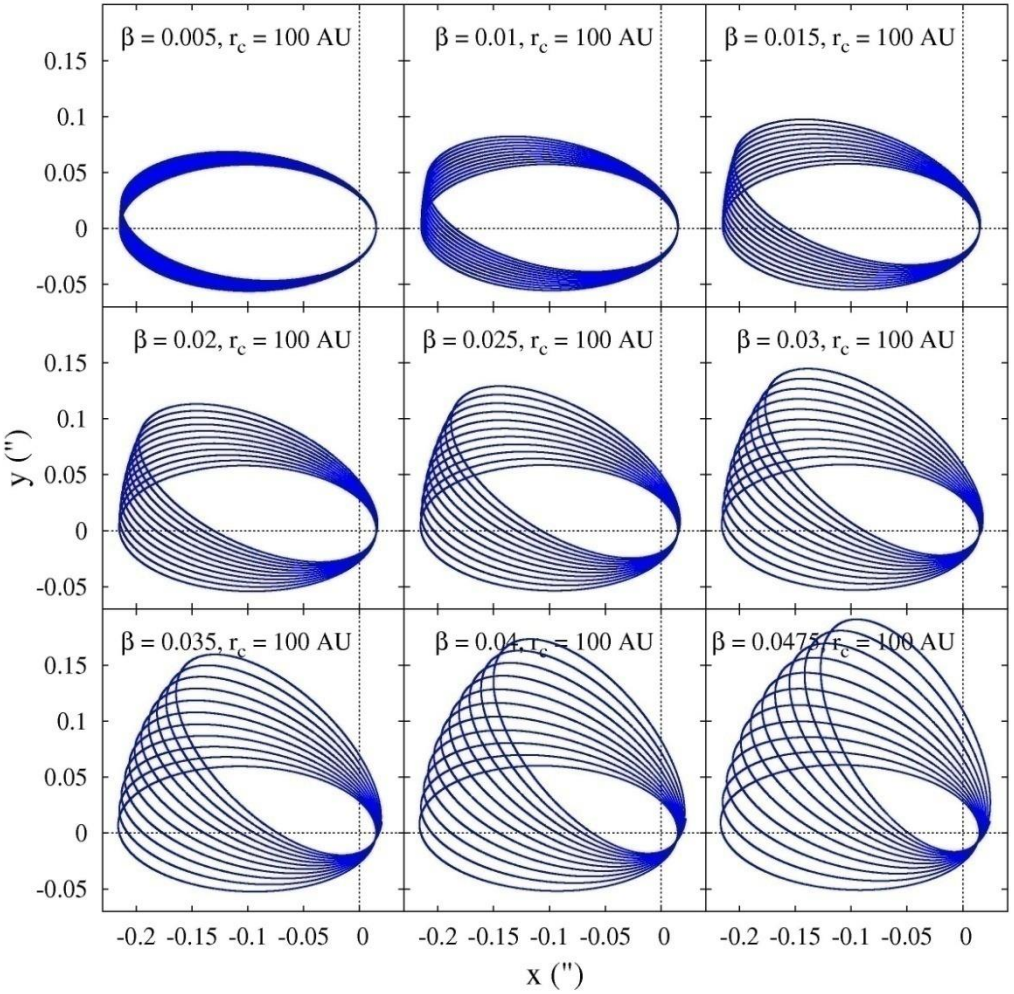

capabilities. They showed that the orbital precession can occur due to relativistic effects, resulting in a prograde shift and due to a possible extended mass distribution, producing a retrograde shift. Both prograde relativistic and retrograde Newtonian periastron shifts will result in rosette-shaped orbits. Weinberg *et al.* [12] discussed physical experiments achievable via the monitoring of stellar dynamics near the massive black hole at the Galactic center with a diffraction-limited, next-generation, extremely large telescope. They demonstrated that the lowest order relativistic effects, such as the prograde precession, will be detectable if the astrometric precision becomes less than 0.5 mas.

In this paper we continue to investigate constraints on the parameters of this class of gravity theories using S2-like star orbits under the uncertainty of 10 mas. In Sec. II the type of gravitational potential we use is given. In Sec. III we present the S2-like star orbits, gravity parameters, and angles of orbital precession, and also compare theoretical results with observations. The main conclusions are pointed out in Sec. IV.

II. THEORY

R^n gravity belongs to power-law fourth-order theories of gravity obtained by replacing the scalar curvature R with $f(R) = f_0 R^n$ in the gravity Lagrangian [1,2]. As a result, in the weak field limit [13], the gravitational potential is found to be [1,2]

$$\Phi(r) = -\frac{GM}{2r}\left[1 + \left(\frac{r}{r_c}\right)^{\beta}\right], \tag{1}$$

where r_c is an arbitrary parameter, depending on the typical scale of the considered system, and β is a universal parameter:

$$\beta = \frac{12n^2 - 7n - 1 - \sqrt{36n^4 + 12n^3 - 83n^2 + 50n + 1}}{6n^2 - 4n + 2}. \tag{2}$$

This formula corresponds to a modification of the gravity action in the form

$$A = \int d^4x\sqrt{-g}(f(R) + L_m), \tag{3}$$

where $f(R)$ is a generic function of the Ricci scalar curvature and L_m is the standard matter Lagrangian.

For $n = 1$ and $\beta = 0$ the R^n potential reduces to the Newtonian one, as expected. Parameter β controls the shape of the correction term and is related to n, which is part of the gravity Lagrangian. Since it is the same for all gravitating systems, as a consequence, β must be the same for all of them and therefore it is a universal parameter [2]. The parameter r_c is the scale length parameter, and it is related to the boundary conditions and the mass of the system [2].

III. RESULTS

A. Orbits of S2-like stars and parameters of R^n gravity

In order to study the effects of R^n gravity on the motion of S2, we performed two-body calculations of its orbit in the R^n potential [Eq. (1)] during two periods. We assumed the following input parameters taken from the paper of Zakharov *et al.* [10]: orbital eccentricity of the S2-like star, $e = 0.87$; major semiaxis $a = 919$ AU; mass of the S2-like star, $M_\star = 1M_\odot$; mass of the central black hole, $M_{\rm BH} = 3.4 \times 10^6 M_\odot$ (where $M_\odot$ is the solar mass); and orbital period of the S2-like star is 15 years. We calculated the S2-like star orbit during two periods using Newtonian and R^n potentials. We also investigated the constraints on the parameters β and r_c for which the deviations between the S2-like star orbits in the R^n gravity potential [Eq. (1)] and its Keplerian orbit will stay within the maximum precision of the current instruments (about 10 mas), during one orbital period.

In Fig. 1 we present the trajectory of the S2-like star around a massive black hole in R^n gravity (blue solid line) and in Newtonian gravity (red dashed line) for $r_c =$ 100 AU and for the following nine values of parameter β: 0.005, 0.01, 0.015, 0.02, 0.025, 0.03, 0.035, 0.04, 0.0475. The black hole is assumed to be located at the coordinate origin. We fix a value of parameter r_c at 100 AU, because this value corresponds to the maximal value of parameter β in the parameter space (see Fig. 3), and vary values of parameter β. All nine orbits presented fulfill the request that the R^n orbit and the corresponding Newtonian orbit differ by less than 10 mas (i.e. within the maximum precision of the current observations) during one orbital period. We can see that if parameter β increases, the R^n orbit differs more from the corresponding Newtonian orbit since the precession angle becomes larger. This indicates that the value of β should be small, as inferred from Solar System data [9] and in contrast to the value $\beta = 0.817$ (obtained by [2], which gives excellent agreement between theoretical and observed rotation curves). In the future, with improvements in observational facilities, the precision on constraints on values of parameters β and r_c will increase, as will the accuracy of the S2 orbit.

The corresponding distances between the S2-like star and the black hole as a function of time for the same values of parameters r_c and β as in Fig. 1 are presented in Fig. 2. There is an additional requirement on parameter space: the period of the S2-like star orbit has to remain $\approx$ 15 ± 0.2 yr. Like in the previous case, with increasing observational accuracy of the period, the precision on constraints on values of parameters β and r_c will also increase.

In Fig. 3 we present the parameter space for R^n gravity under the constraint that, during one orbital period, S2-like star orbits under R^n gravity differ by less than ε from their orbits under Newtonian gravity for ten values of parameter ε: 0.001, 0.002, 0.003, 0.004, 0.005, 0.006, 0.007, 0.008,

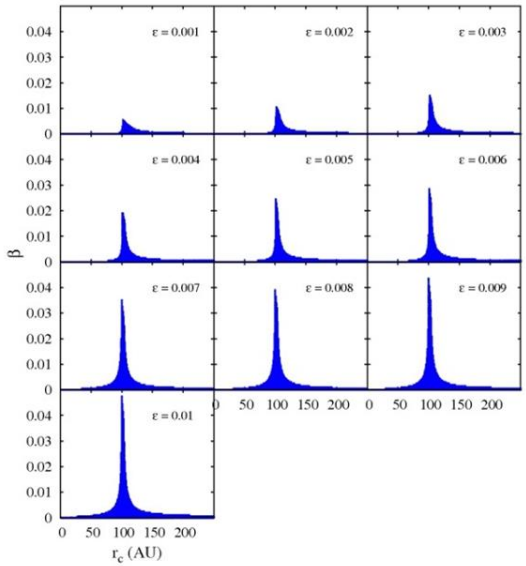

FIG. 3 (color online). The parameter space for R^n gravity under the constraint that, during one orbital period, the S2-like star orbits in R^n gravity differ by less than ε from the corresponding orbits in Newtonian gravity, for the following ten values of parameter ε: 0.001, 0.002, 0.003, 0.004, 0.005, 0.006, 0.007, 0.008, 0.009, and $0''.01$.

The exact expression (7) is inappropriate for practical applications. However, it can be easily approximated for $\beta \approx 0$ and $\beta \approx 1$. In the case of $\beta \approx 0$ expansion in Eq. (7) in Taylor's series over β, up to first order, leads to the following expression for the precession angle:

$$\Delta\theta = \frac{\pi^{\mathrm{rad}}\beta(\sqrt{1-e^2}-1)}{e^2} = \frac{180^\circ\beta(\sqrt{1-e^2}-1)}{e^2}. \quad (8)$$

The above expression in the case of the S2-like star orbit is presented in Fig. 9 as a blue dash-dotted line. Similarly, the expansion of Eq. (7) in power series for $\beta \approx 1$ leads to the following expression for the precession angle (red dotted line in Fig. 9):

$$\Delta\theta = \frac{\pi^{\mathrm{rad}}a(\beta-1)(\sqrt{1-e^2}-1+e^2)}{r_c e^2} = \frac{180^\circ a(\beta-1)(\sqrt{1-e^2}-1+e^2)}{r_c e^2}. \quad (9)$$

One can expect that, in general, the precession angle depends on the semimajor axis and eccentricity of the orbit (see e.g. Iorio and Ruggiero [17]), as well as on both potential parameters β and r_c. This is indeed the case for $\beta \approx 1$ in Eq. (9). But as it can be seen from formula (8), the precession angle in the case when β is small ($\beta \approx 0$) depends only on the eccentricity and the universal constant β itself.

In order to test if the approximation from Eq. (8) is satisfactory in the case of the S2-like star, we derived its precession angle in two ways:

(i) analytically from the approximative formula (8),
(ii) numerically from the calculated orbits presented in Fig. 8.

Comparison of the obtained precession angles by these two methods is presented in Table I. As it can be seen from this table, the approximative formula (8) can be used for estimating the precession angle for all values of β from Fig. 8.

The above analysis indicates that R^n gravity results in the retrograde shift of the S2-like star orbit. Rubilar and Eckart [11] showed that the orbital precession can be due to relativistic effects, resulting in a prograde shift, or due to an extended mass distribution, producing a retrograde shift. We can conclude that the perturbing potential $V(r)$ has an

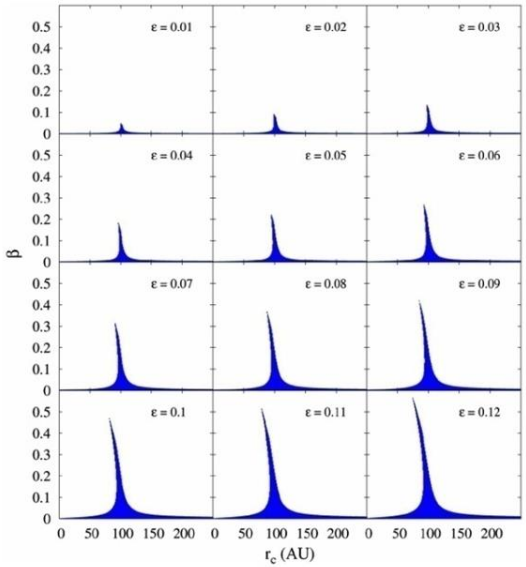

FIG. 4 (color online). The same as in Fig. 3 but for the following 12 values of parameter ε: 0.01, 0.02, 0.03, 0.04, 0.05, 0.06, 0.07, 0.08, 0.09, 0.1, 0.11, and $0''.12$.

effect similar to extended mass distribution, since it produces a retrograde orbital shift.

Since the precession has a negative direction, as in the case of extended mass distribution, the obtained results are useful for testing if the precession due to extended dark matter enclosed in the orbit of an S2-like star could also be explained by R^n gravity. If this is possible, it will exclude the need for a dark matter hypothesis. Therefore, if future and more precise observations of bright stars near the Galactic center show a precession in the negative direction, we have to conclude that the phenomenon could be caused by bulk distributions of stellar clusters and/or dark matter in classical Newtonian (GR) gravity or by R^n gravity. On the other hand, if there are no deviations from Newtonian (GR) trajectories with an accuracy of observations, one could put constraints on stellar cluster and dark matter

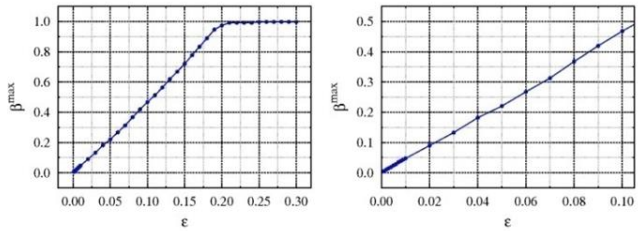

FIG. 5 (color online). The dependence of the maximal value of parameter β on precision ε ranging from 0 to $0''.3$ (left panel) and from 0 to $0''.1$ (right panel).

D. Borka, V. Borka Jovanovic, P. Jovanovic, AFZ

From an analysis of S2 orbit one can find signatures of Yukawa gravity (JCAP, 2013)

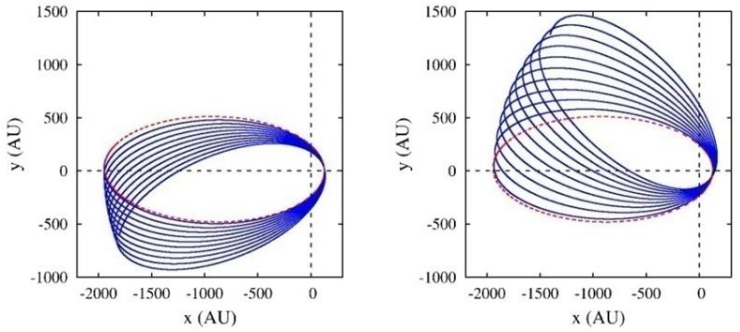

Figure 1. Comparisons between the orbit of S2 star in Newtonian gravity (red dashed line) and Yukawa gravity during 10 orbital periods (blue solid line) for $\Lambda = 2.59 \times 10^3$ AU. In the left panel $\delta = +1/3$, and in the right $\delta = -1/3$.

5. the reduced χ^2 is minimized and the final values of initial positions and velocities are obtained.

Finally, we kept the value of Λ which resulted with the smallest value of minimized reduced χ^2.

In order to obtain some more general constraints on the parameters of Yukawa gravity, we also varied both δ and Λ and studied the simulated orbits of S2 star which give at least the same or better fits than the Keplerian orbit. For each pair of these parameters the reduced χ^2 of the best fit is obtained and used for generating the χ^2 maps over the $\Lambda - \delta$ parameter space. These maps are then used to study the confidence regions in $\Lambda - \delta$ parameter space.

3 Results and discussion

The simulated orbits of S2 star around the central object in Yukawa gravity (blue solid line) and in Newtonian gravity (red dashed line) for $\Lambda = 2.59 \times 10^3$ AU and $\delta = +1/3$ (left panel) and $\delta = -1/3$ (right panel) during 10 periods, are presented in Fig. 1. We can notice that for $\delta = -1/3$ the precession has negative direction and when $\delta = +1/3$ the precession has positive direction. Our analysis shows that the Yukawa gravity potential induces precession of S2 star orbit in the same direction as General Relativity for $\delta > 0$ and for $\delta < -1$, and in the opposite direction for $-1 < \delta < 0$ as in the case of extended mass distribution or in R^n gravity [22].

We used these simulated orbits to fit the observed orbits of S2 star. The best fit (according to NTT/VLT data) is obtained for the scale parameter: $\Lambda = 2.59 \times 10^3$ AU, for which even a significant strength of Yukawa interaction could be expected according to the planetary and Lunar Laser Ranging constraints [32].

In Fig. 2 we presented two comparisons between the fitted orbits in Yukawa gravity for $\delta = +1/3$ through the astrometric observations of S2 star by NTT/VLT alone (left) and NTT/VLT+Keck combination (right). In order to combine NTT/VLT and Keck data sets,

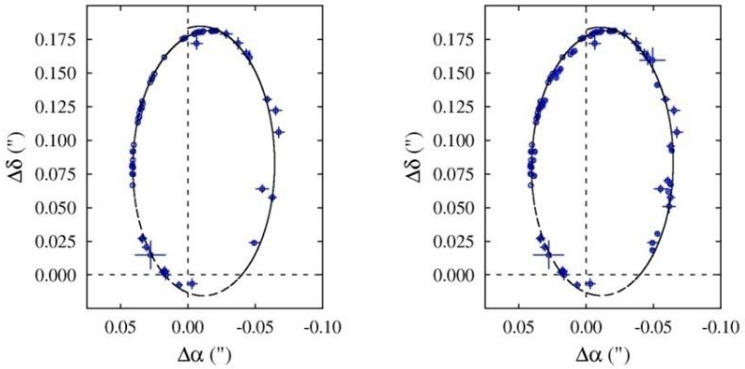

Figure 2. The fitted orbits in Yukawa gravity for $\delta = +1/3$ through the astrometric observations of S2 star (denoted by circles), obtained by NTT/VLT alone (left panel) and NTT/VLT+Keck (right panel). The best fits are obtained for $\Lambda = 2.59 \times 10^3$ AU and $\Lambda = 3.03 \times 10^3$ AU, respectively.

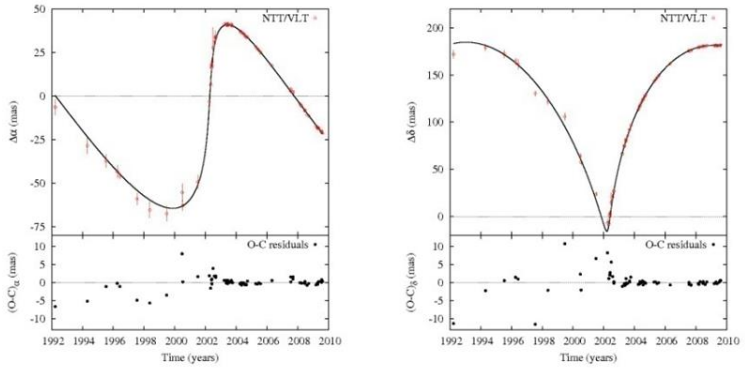

Figure 3. The comparisons between the observed (open circles with error bars) and fitted (solid lines) coordinates of S2 star (top), as well as the corresponding O-C residuals (bottom). The left panel shows the results for $\Delta\alpha$ and right panel for $\Delta\delta$ in the case of NTT/VLT observations and Yukawa gravity potential with $\delta = +1/3$ and $\Lambda = 2.59 \times 10^3$ AU.

the position of the origin of Keck observations is first shifted by $\Delta x = 3.7$ and $\Delta y = 4.1$ mas, following the suggestion given in [39]. In the first case the best fit is obtained for $\Lambda = 2.59 \times 10^3$ AU, resulting with reduced $\chi^2 = 1.54$, and in the second case for $\Lambda = 3.03 \times 10^3$ AU with reduced $\chi^2 = 3.24$. As one can see from these figures, in both cases there is a good agreement between the theoretical orbits and observations, although the higher value of reduced χ^2 in

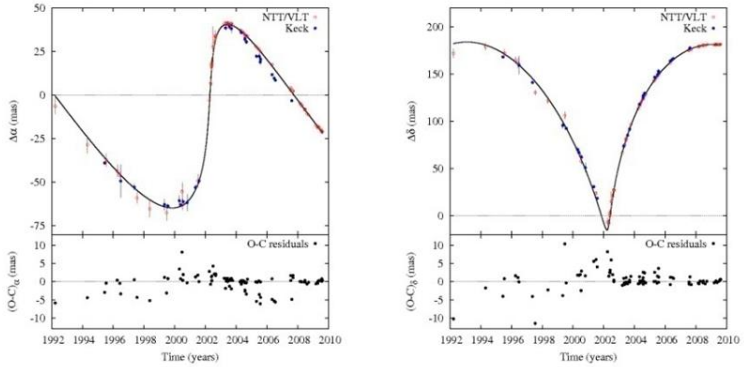

Figure 4. The same as in Fig. 3, but for NTT/VLT+Keck combined observations and for Yukawa gravity potential with $\Lambda = 3.03 \times 10^3$ AU.

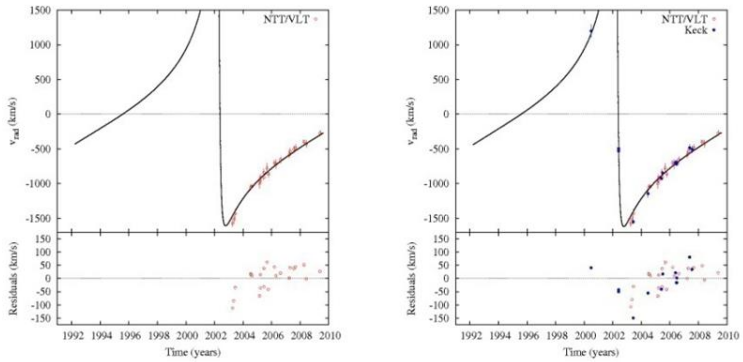

Figure 5. The comparisons between the observed (circles with error bars) and fitted (solid lines) radial velocities of S2 star (top), as well as the corresponding O-C residuals (bottom). The left panel shows the results in the case of NTT/VLT observations and Yukawa gravity potential with $\Lambda = 2.59 \times 10^3$ AU, while the right panel shows the results for NTT/VLT+Keck combined observations and for Yukawa gravity potential with $\Lambda = 3.03 \times 10^3$ AU. In both cases $\delta = +1/3$.

the second case indicates possibly larger positional difference between the two coordinate systems, as also noted in [39]. These figures also show that the simulated orbits of S2 are not closed in vicinity of apocenter, indicating a possible orbital precession.

In Figs. 3 and 4 we presented the comparisons between the observed and fitted coordinates of S2 star and their O-C residuals in the case of NTT/VLT observations, as well as NTT/VLT+Keck combined data set, respectively. One can notice that in both cases, O-C

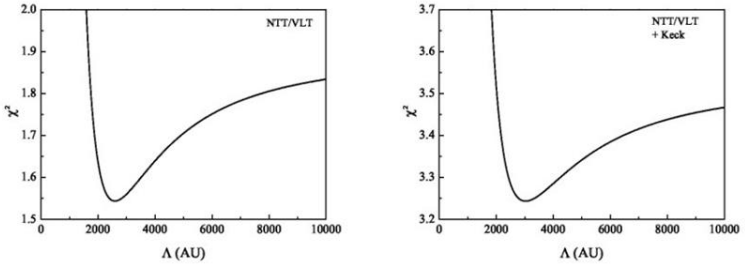

Figure 6. The reduced χ^2 for δ=1/3 as a function of Λ in case of NTT/VLT alone (left) and combined NTT/VLT+Keck (right) observations.

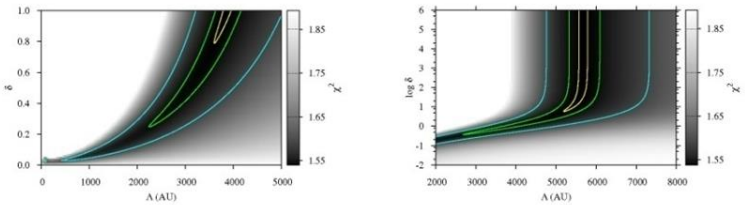

Figure 7. The maps of reduced χ^2 over the $\Lambda - \delta$ parameter space in case of NTT/VLT observations. The left panel corresponds to $\delta \in [0, 1]$, and the right panel to the extended range of $\delta \in [0.01, 10^6]$. The shades of gray color represent the values of the reduced χ^2 which are less than the corresponding value in the case of Keplerian orbit, and three contours (from inner to outer) enclose the confidence regions in which the difference between the current and minimum reduced χ^2 is less than 0.0005, 0.005 and 0.05, respectively.

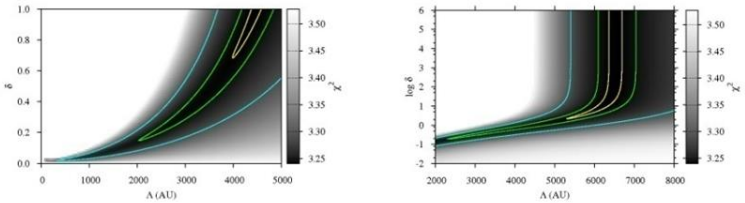

Figure 8. The same as in Fig. 7, but for the combined NTT/VLT+Keck observations.

residuals are higher in the first part of observing interval (up to the 12 mas) and much less in its second part (less than 2 mas). Due to adopted merit function given by expression (2.7), our fitting procedure assigned greater weight to these latter, more precise observations. Also, the O-C residuals are larger in the case of the combined NTT/VLT+Keck observations most likely due to the shift of the origin of the coordinate system, which was necessary in order to

Massive graviton theories

- M. Fierz and W.Pauli-1939
- Zakharov; Veltman, van Dam – 1970
- Vainshtein - 1972
- Boulware, Deser -- 1972
- Logunov, Mestvirishvili, Gershtein et al.
- Visser – 1998 (review on such theories)
- Rubakov, Tinyakov – 2008
- DeRham --2016

Massive graviton theories (constraints)

- A. S. Goldhaber and M. M. Nieto (2010): model dependent astrophysical constraints
- C. Will – 1998, 2014
- $V(r) = (GM/r) \exp(-r/\lambda_g)$
- $\lambda_g > 2.8 \times 10^{12}$ km (Will, 1998, 2014) from GW signal, delays, chirp

Graviton Mass Estimate from Gravitational Wave Signal

If a graviton has a mass m_g, then in this case a speed of gravitational wave propagation could differ from c and we have a dispersion relation (Will, 1998)

$$\frac{v_g^2}{c^2} = 1 - \frac{m_g^2 c^4}{E^2}, \tag{1}$$

where E is a graviton energy. Gravitons with different energies propagate with different velocities. Assume that we have gravitational waves and electromagnetic waves from the same source (from supernovae exoplosion, for instance). In this case we have (Will, 1998)

$$1 - \frac{v_g}{c} = 5 \times 10^{-17} \left(\frac{200 \text{ Mpc}}{D}\right) \left(\frac{\Delta t}{1 \text{ s}}\right), \tag{2}$$

where $\Delta t = \Delta t_a - (1+z)\Delta t_e$ is the time difference, where Δt_a and Δt_e are the differences in arrival time and emission time of the two signals, respectively, and z is the redshift of the source. Usually Δt_e is unknown, however, one could find an upper limit for Δt_e (for instance from a theoretical model), therefore, one could evaluate $1 - \frac{v_g}{c}$, therefore, m_g. Following (Will, 1998) and assuming that the frequency of gravitational wave is ν and $h\nu \gg m_g c^2$ (h is Planck's constant), therefore, we have $\frac{v_g}{c} \approx 1 - \frac{1}{2}\frac{h}{\lambda_g \nu}$, where $\lambda_g = \frac{h}{m_g c}$ or $\lambda_g \approx \frac{1}{2}\frac{1}{\sqrt{1 - v_g/c}}$. If one has an upper limit for $1 - v_g/c$, it can be re-written as a lower limit for λ_g, as the following expression (Will, 1998)

$$\lambda_g = 3 \times 10^{12} \mathrm{km} \left(\frac{200\ \mathrm{Mpc}}{D} \frac{\nu}{100 \mathrm{Hz}} \right) \left(\frac{1}{\nu \Delta t} \right). \tag{3}$$

It is a lucky case if one observe electromagnetic and gravitational radiation

from the same source. But even in the case if only gravitational radiation has been detected as it was noted by Will (1998) because gravitational wave signal with a massive graviton will be different from signal for a graviton with a vanishing mass and in this case for $D \approx 200\mathrm{Mpc}, \nu \approx 100\mathrm{Hz}, \nu\Delta t \sim \rho^{-1} \approx 0.1$ The result is $\lambda_g > 10^{13}$ km. Based on ideas expressed in (Will, 1998), the LIGO/VIRGO collaboration obtained the same estimate for the Compton wavelength of a massive graviton (Abbott et al. (LIGO) 2016).

Observation of Gravitational Waves from a Binary Black Hole Merger

B. P. Abbott *et al.*[*]
(LIGO Scientific Collaboration and Virgo Collaboration)
(Received 21 January 2016; published 11 February 2016)

On September 14, 2015 at 09:50:45 UTC the two detectors of the Laser Interferometer Gravitational-Wave Observatory simultaneously observed a transient gravitational-wave signal. The signal sweeps upwards in frequency from 35 to 250 Hz with a peak gravitational-wave strain of 1.0×10^{-21}. It matches the waveform predicted by general relativity for the inspiral and merger of a pair of black holes and the ringdown of the resulting single black hole. The signal was observed with a matched-filter signal-to-noise ratio of 24 and a false alarm rate estimated to be less than 1 event per 203 000 years, equivalent to a significance greater than 5.1σ. The source lies at a luminosity distance of 410^{+160}_{-180} Mpc corresponding to a redshift $z = 0.09^{+0.03}_{-0.04}$. In the source frame, the initial black hole masses are $36^{+5}_{-4} M_\odot$ and $29^{+4}_{-4} M_\odot$, and the final black hole mass is $62^{+4}_{-4} M_\odot$, with $3.0^{+0.5}_{-0.5} M_\odot c^2$ radiated in gravitational waves. All uncertainties define 90% credible intervals. These observations demonstrate the existence of binary stellar-mass black hole systems. This is the first direct detection of gravitational waves and the first observation of a binary black hole merger.

DOI: 10.1103/PhysRevLett.116.061102

I. INTRODUCTION

In 1916, the year after the final formulation of the field equations of general relativity, Albert Einstein predicted the existence of gravitational waves. He found that the linearized weak-field equations had wave solutions: transverse waves of spatial strain that travel at the speed of light, generated by time variations of the mass quadrupole moment of the source [1,2]. Einstein understood that gravitational-wave amplitudes would be remarkably small; moreover, until the Chapel Hill conference in 1957 there was significant debate about the physical reality of gravitational waves [3].

Also in 1916, Schwarzschild published a solution for the field equations [4] that was later understood to describe a black hole [5,6], and in 1963 Kerr generalized the solution to rotating black holes [7]. Starting in the 1970s theoretical work led to the understanding of black hole quasinormal modes [8–10], and in the 1990s higher-order post-Newtonian calculations [11] preceded extensive analytical studies of relativistic two-body dynamics [12,13]. These advances, together with numerical relativity breakthroughs in the past decade [14–16], have enabled modeling of binary black hole mergers and accurate predictions of their gravitational waveforms. While numerous black hole candidates have now been identified through electromagnetic observations [17–19], black hole mergers have not previously been observed.

The discovery of the binary pulsar system PSR B1913+16 by Hulse and Taylor [20] and subsequent observations of its energy loss by Taylor and Weisberg [21] demonstrated the existence of gravitational waves. This discovery, along with emerging astrophysical understanding [22], led to the recognition that direct observations of the amplitude and phase of gravitational waves would enable studies of additional relativistic systems and provide new tests of general relativity, especially in the dynamic strong-field regime.

Experiments to detect gravitational waves began with Weber and his resonant mass detectors in the 1960s [23], followed by an international network of cryogenic resonant detectors [24]. Interferometric detectors were first suggested in the early 1960s [25] and the 1970s [26]. A study of the noise and performance of such detectors [27], and further concepts to improve them [28], led to proposals for long-baseline broadband laser interferometers with the potential for significantly increased sensitivity [29–32]. By the early 2000s, a set of initial detectors was completed, including TAMA 300 in Japan, GEO 600 in Germany, the Laser Interferometer Gravitational-Wave Observatory (LIGO) in the United States, and Virgo in Italy. Combinations of these detectors made joint observations from 2002 through 2011, setting upper limits on a variety of gravitational-wave sources while evolving into a global network. In 2015, Advanced LIGO became the first of a significantly more sensitive network of advanced detectors to begin observations [33–36].

A century after the fundamental predictions of Einstein and Schwarzschild, we report the first direct detection of gravitational waves and the first direct observation of a binary black hole system merging to form a single black hole. Our observations provide unique access to the

[*]Full author list given at the end of the article.

properties of space-time in the strong-field, high-velocity regime and confirm predictions of general relativity for the nonlinear dynamics of highly disturbed black holes.

II. OBSERVATION

On September 14, 2015 at 09:50:45 UTC, the LIGO Hanford, WA, and Livingston, LA, observatories detected the coincident signal GW150914 shown in Fig. 1. The initial detection was made by low-latency searches for generic gravitational-wave transients [41] and was reported within three minutes of data acquisition [43]. Subsequently, matched-filter analyses that use relativistic models of compact binary waveforms [44] recovered GW150914 as the most significant event from each detector for the observations reported here. Occurring within the 10-ms intersite

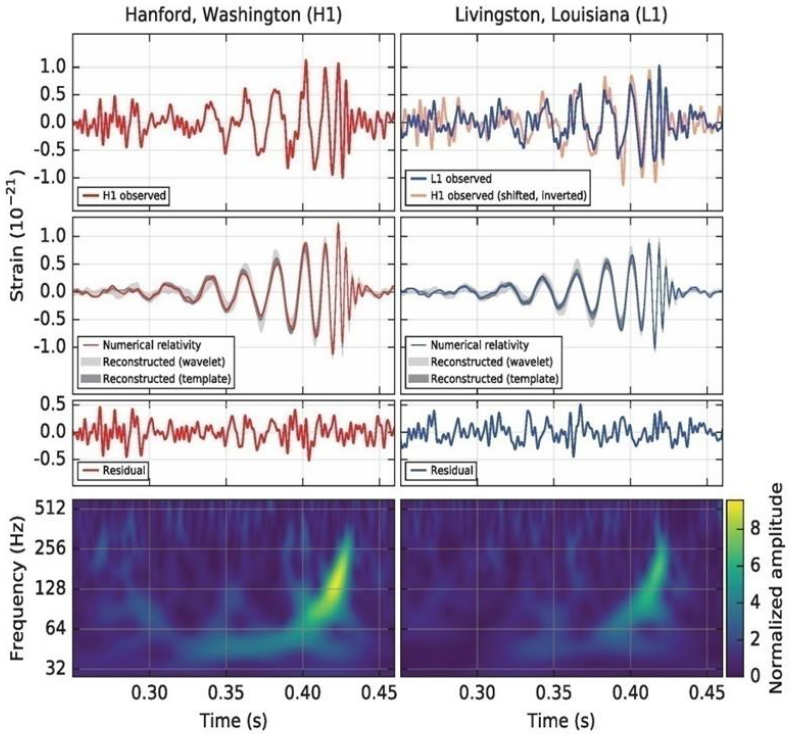

FIG. 1. The gravitational-wave event GW150914 observed by the LIGO Hanford (H1, left column panels) and Livingston (L1, right column panels) detectors. Times are shown relative to September 14, 2015 at 09:50:45 UTC. For visualization, all time series are filtered with a 35–350 Hz bandpass filter to suppress large fluctuations outside the detectors' most sensitive frequency band, and band-reject filters to remove the strong instrumental spectral lines seen in the Fig. 3 spectra. *Top row, left:* H1 strain. *Top row, right:* L1 strain. GW150914 arrived first at L1 and $6.9^{+0.5}_{-0.4}$ ms later at H1; for a visual comparison, the H1 data are also shown, shifted in time by this amount and inverted (to account for the detectors' relative orientations). *Second row:* Gravitational-wave strain projected onto each detector in the 35–350 Hz band. Solid lines show a numerical relativity waveform for a system with parameters consistent with those recovered from GW150914 [37,38] confirmed to 99.9% by an independent calculation based on [15]. Shaded areas show 90% credible regions for two independent waveform reconstructions. One (dark gray) models the signal using binary black hole template waveforms [39]. The other (light gray) does not use an astrophysical model, but instead calculates the strain signal as a linear combination of sine-Gaussian wavelets [40,41]. These reconstructions have a 94% overlap, as shown in [39]. *Third row:* Residuals after subtracting the filtered numerical relativity waveform from the filtered detector time series. *Bottom row:*A time-frequency representation [42] of the strain data, showing the signal frequency increasing over time.

propagation time, the events have a combined signal-to-noise ratio (SNR) of 24 [45].

Only the LIGO detectors were observing at the time of GW150914. The Virgo detector was being upgraded, and GEO 600, though not sufficiently sensitive to detect this event, was operating but not in observational mode. With only two detectors the source position is primarily determined by the relative arrival time and localized to an area of approximately 600 deg^2 (90% credible region) [39,46].

The basic features of GW150914 point to it being produced by the coalescence of two black holes—i.e., their orbital inspiral and merger, and subsequent final black hole ringdown. Over 0.2 s, the signal increases in frequency and amplitude in about 8 cycles from 35 to 150 Hz, where the amplitude reaches a maximum. The most plausible explanation for this evolution is the inspiral of two orbiting masses, m_1 and m_2, due to gravitational-wave emission. At the lower frequencies, such evolution is characterized by the chirp mass [11]

$$\mathcal{M} = \frac{(m_1 m_2)^{3/5}}{(m_1 + m_2)^{1/5}} = \frac{c^3}{G}\left[\frac{5}{96}\pi^{-8/3} f^{-11/3}\dot{f}\right]^{3/5},$$

where f and $\dot{f}$ are the observed frequency and its time derivative and G and c are the gravitational constant and speed of light. Estimating f and $\dot{f}$ from the data in Fig. 1, we obtain a chirp mass of $\mathcal{M} \simeq 30 M_\odot$, implying that the total mass $M = m_1 + m_2$ is $\gtrsim 70 M_\odot$ in the detector frame. This bounds the sum of the Schwarzschild radii of the binary components to $2GM/c^2 \gtrsim 210$ km. To reach an orbital frequency of 75 Hz (half the gravitational-wave frequency) the objects must have been very close and very compact; equal Newtonian point masses orbiting at this frequency would be only $\simeq$350 km apart. A pair of neutron stars, while compact, would not have the required mass, while a black hole neutron star binary with the deduced chirp mass would have a very large total mass, and would thus merge at much lower frequency. This leaves black holes as the only known objects compact enough to reach an orbital frequency of 75 Hz without contact. Furthermore, the decay of the waveform after it peaks is consistent with the damped oscillations of a black hole relaxing to a final stationary Kerr configuration. Below, we present a general-relativistic analysis of GW150914; Fig. 2 shows the calculated waveform using the resulting source parameters.

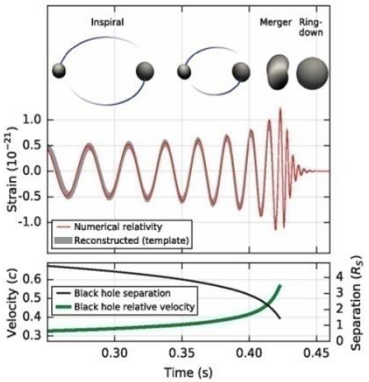

FIG. 2. *Top:* Estimated gravitational-wave strain amplitude from GW150914 projected onto H1. This shows the full bandwidth of the waveforms, without the filtering used for Fig. 1. The inset images show numerical relativity models of the black hole horizons as the black holes coalesce. *Bottom:* The Keplerian effective black hole separation in units of Schwarzschild radii ($R_S = 2GM/c^2$) and the effective relative velocity given by the post-Newtonian parameter $v/c = (GM\pi f/c^3)^{1/3}$, where f is the gravitational-wave frequency calculated with numerical relativity and M is the total mass (value from Table I).

III. DETECTORS

Gravitational-wave astronomy exploits multiple, widely separated detectors to distinguish gravitational waves from local instrumental and environmental noise, to provide source sky localization, and to measure wave polarizations. The LIGO sites each operate a single Advanced LIGO detector [33], a modified Michelson interferometer (see Fig. 3) that measures gravitational-wave strain as a difference in length of its orthogonal arms. Each arm is formed by two mirrors, acting as test masses, separated by $L_x = L_y = L = 4$ km. A passing gravitational wave effectively alters the arm lengths such that the measured difference is $\Delta L(t) = \delta L_x - \delta L_y = h(t)L$, where h is the gravitational-wave strain amplitude projected onto the detector. This differential length variation alters the phase difference between the two light fields returning to the beam splitter, transmitting an optical signal proportional to the gravitational-wave strain to the output photodetector.

To achieve sufficient sensitivity to measure gravitational waves, the detectors include several enhancements to the basic Michelson interferometer. First, each arm contains a resonant optical cavity, formed by its two test mass mirrors, that multiplies the effect of a gravitational wave on the light phase by a factor of 300 [48]. Second, a partially transmissive power-recycling mirror at the input provides additional resonant buildup of the laser light in the interferometer as a whole [49,50]: 20 W of laser input is increased to 700 W incident on the beam splitter, which is further increased to 100 kW circulating in each arm cavity. Third, a partially transmissive signal-recycling mirror at the output optimizes

- One of the goals of advanced LIGO, VIRGO is not only GW's detection but also to obtain constraints on graviton mass (Will, 2014)
- $m_g < 1.2 \times 10^{-22}$ eV (see, B. P. Abbott et al. (LIGO Scientific Collaboration and Virgo Collaboration), PRL 116, 061102 (2016))

May 4, 2016 -- The Gruber Foundation has announced the award of the 2016 Gruber Cosmology Prize to LIGO's Ronald W.P. Drever (Caltech), Kip S. Thorne (Caltech), and Rainer Weiss (MIT) for the detection of gravitational waves.

Massive graviton theories (constraints)

- Sazhin (1978) GW's could be detected with pulsar timing
- Lee et al. (2010) array of pulsars and timing 60 pulsars – 5 years with accuracy 100 ns -- $\lambda_g > 4 \times 10^{12}$ km
-

Graviton Mass Estimates from Trajectories of Bright Stars near the Galactic Center

We use a modification of the Newtonian potential corresponding to a massive graviton case (Will, 1998):

$$V(r) = -\frac{GM}{(1+\delta)r}\left[1 + \delta e^{-\left(\frac{r}{\lambda}\right)}\right], \tag{4}$$

where δ is a universal constant (we put $\delta = 1$). In our previous studies [**?**] we found constraints on parameters of Yukawa gravity. As it was described in (Zakharov et al. 2016) we used observational data from VLT. If we wish to find a limiting value for λ_x, so that $\lambda > \lambda_x$ with a probability

$P = 1 - \alpha$ (where we select $\alpha = 0.1$) normalized χ^2 depending on λ_x has to be equal to the threshold depending on degree of freedom ν and parameter α or in other words, $\chi^2(\lambda_x) = \chi^2_{\nu,\alpha}$. Computing these quantities we obtain $\lambda_x = 2900$ AU $\approx 4.3 \times 10^{11}$ km. Now we obtain the upper limit on a graviton mass and we could claim that with a probability $P = 0.9$, a graviton mass should be less than $m_g = 2.9 \times 10^{-21}$ eV (since $m_g = h\,c/\lambda_x$) in the case of $\delta = 1$ (Zakharov et al. 2016).

- S.S. Gershtein , A.A. Logunov , M.A. Mestvirishvili, N.P. Tkachenko (PAN, 2003):
- m_g =1.3 x 10^{-66} g (no contradiction with LIGO
- and our estimates)
- S.S. Gershtein, A.A. Logunov, M.A. Mestvirishvili (Doklady-Physics, 2003)
- m_g =3.2 x 10^{-66} g (95% c.l.)

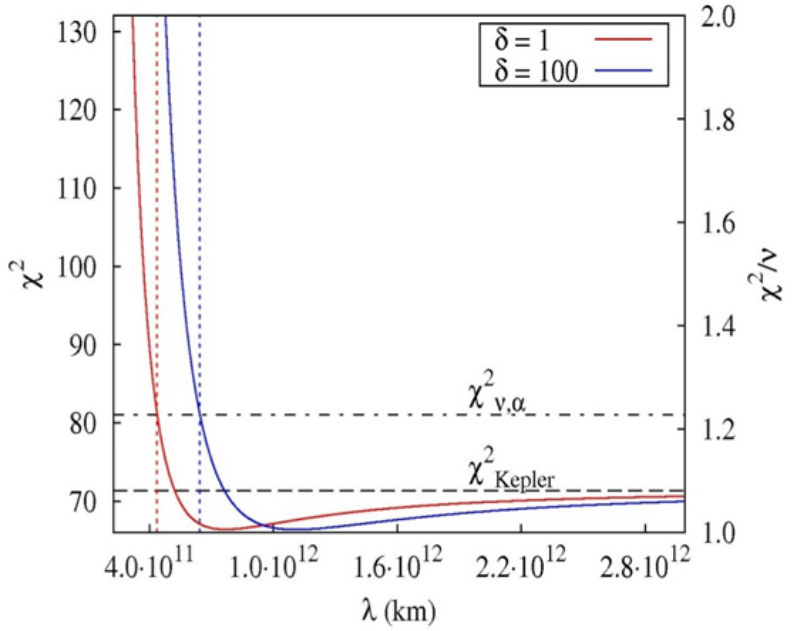
δ = 1
δ = 100
χ²
χ²/ν
χ²ν,α
χ²Kepler
130
120
110
100
90
80
70
2.0
1.8
1.6
1.4
1.2
1.0
4.0·10¹¹
1.0·10¹²
1.6·10¹²
2.2·10¹²
2.8·10¹²
λ (km)

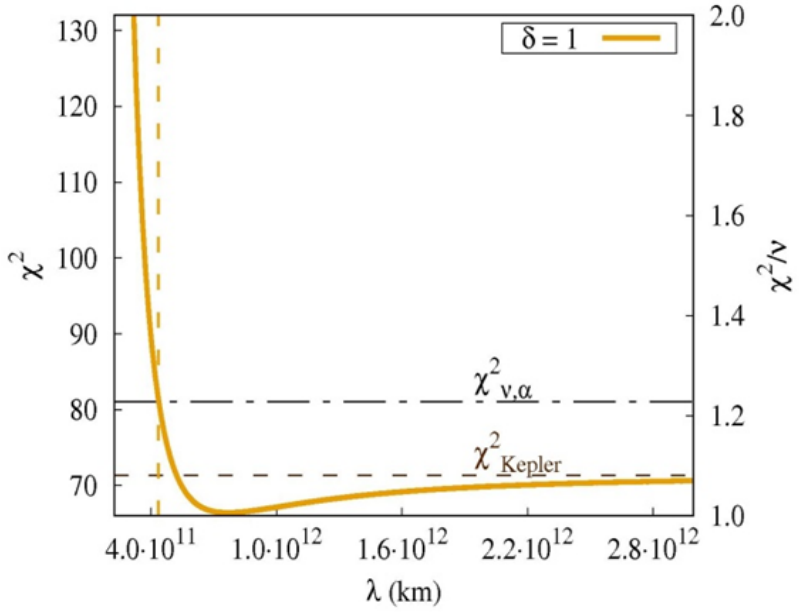
δ = 1
χ²
χ²/ν
χ²ν,α
χ²Kepler
130
120
110
100
90
80
70
2.0
1.8
1.6
1.4
1.2
1.0
4.0·10¹¹
1.0·10¹²
1.6·10¹²
2.2·10¹²
2.8·10¹²
λ (km)

Impact on our studies

Claudia de Rham, J. Tate Deskins, Andrew J. Tolley, Shuang-Yong Zhou, Graviton Mass Bounds, Reviews in Modern Physics 89, 0250004 (2017).

A. Hees, T. Do, A. M. Ghez, G. D. Martinez, S. Naoz, E. E. Becklin, A. Boehle, S. Chappell, D. Chu, A. Dehghanfar, K. Kosmo, J. R. Lu, K. Matthews, M. R. Morris, S. Sakai, R. Schodel, and G. Witze, Testing General Relativity with stellar orbits around the supermassive black hole in our Galactic center, arXiv:1705.07902v1 [astro-ph.GA], PRL 118, 211101.

A couple of our papers have been quoted in the second paper.

GW170104: Observation of a 50-Solar-Mass Binary Black Hole Coalescence at Redshift 0.2

B. P. Abbott *et al.*[*]
(LIGO Scientific and Virgo Collaboration)
(Received 9 May 2017; published 1 June 2017)

We describe the observation of GW170104, a gravitational-wave signal produced by the coalescence of a pair of stellar-mass black holes. The signal was measured on January 4, 2017 at 10:11:58.6 UTC by the twin advanced detectors of the Laser Interferometer Gravitational-Wave Observatory during their second observing run, with a network signal-to-noise ratio of 13 and a false alarm rate less than 1 in 70 000 years. The inferred component black hole masses are $31.2^{+8.4}_{-6.0}M_\odot$ and $19.4^{+5.3}_{-5.9}M_\odot$ (at the 90% credible level). The black hole spins are best constrained through measurement of the effective inspiral spin parameter, a mass-weighted combination of the spin components perpendicular to the orbital plane, $\chi_{\rm eff} = -0.12^{+0.21}_{-0.30}$. This result implies that spin configurations with both component spins positively aligned with the orbital angular momentum are disfavored. The source luminosity distance is 880^{+450}_{-390} Mpc corresponding to a redshift of $z = 0.18^{+0.08}_{-0.07}$. We constrain the magnitude of modifications to the gravitational-wave dispersion relation and perform null tests of general relativity. Assuming that gravitons are dispersed in vacuum like massive particles, we bound the graviton mass to $m_g \leq 7.7 \times 10^{-23}$ eV/c^2. In all cases, we find that GW170104 is consistent with general relativity.

DOI: 10.1103/PhysRevLett.118.221101

I. INTRODUCTION

The first observing run of the Advanced Laser Interferometer Gravitational-Wave Observatory (LIGO) [1] identified two binary black hole coalescence signals with high statistical significance, GW150914 [2] and GW151226 [3], as well as a less significant candidate LVT151012 [4,5]. These discoveries ushered in a new era of observational astronomy, allowing us to investigate the astrophysics of binary black holes and test general relativity (GR) in ways that were previously inaccessible [6,7]. We now know that there is a population of binary black holes with component masses $\gtrsim 25M_\odot$ [5,6], and that merger rates are high enough for us to expect more detections [5,8].

Advanced LIGO's second observing run began on November 30, 2016. On January 4, 2017, a gravitational-wave signal was detected with high statistical significance. Figure 1 shows a time-frequency representation of the data from the LIGO Hanford and Livingston detectors, with the signal GW170104 visible as the characteristic chirp of a binary coalescence. Detailed analyses demonstrate that GW170104 arrived at Hanford ~3 ms before Livingston, and originated from the coalescence of two stellar-mass black holes at a luminosity distance of $\sim 3 \times 10^9$ light-years.

GW170104's source is a heavy binary black hole system, with a total mass of $\sim 50M_\odot$, suggesting formation in a subsolar metallicity environment [6]. Measurements of the black hole spins show a preference away from being (positively) aligned with the orbital angular momentum, but do not exclude zero spins. This is distinct from the case for GW151226, which had a strong preference for spins with positive projections along the orbital angular momentum [3]. The inferred merger rate agrees with previous calculations [5,8], and could potentially be explained by binary black holes forming through isolated binary evolution or dynamical interactions in dense stellar clusters [6].

Gravitational-wave observations of binary black holes are the ideal means to test GR and its alternatives. They provide insight into regimes of strong-field gravity where velocities are relativistic and the spacetime is dynamic. The tests performed with the sources detected in the first observing run showed no evidence of departure from GR's predictions [5,7]; GW170104 provides an opportunity to tighten these constraints. In addition to repeating tests performed in the first observing run, we also test for modifications to the gravitational-wave dispersion relation. Combining measurements from GW170104 with our previous results, we obtain new gravitational-wave constraints on potential deviations from GR.

II. DETECTORS AND DATA QUALITY

The LIGO detectors measure gravitational-wave strain using two dual-recycled Fabry-Perot Michelson interferometers at the Hanford and Livingston observatories [1,10].

[*]Full author list given at the end of the Letter.

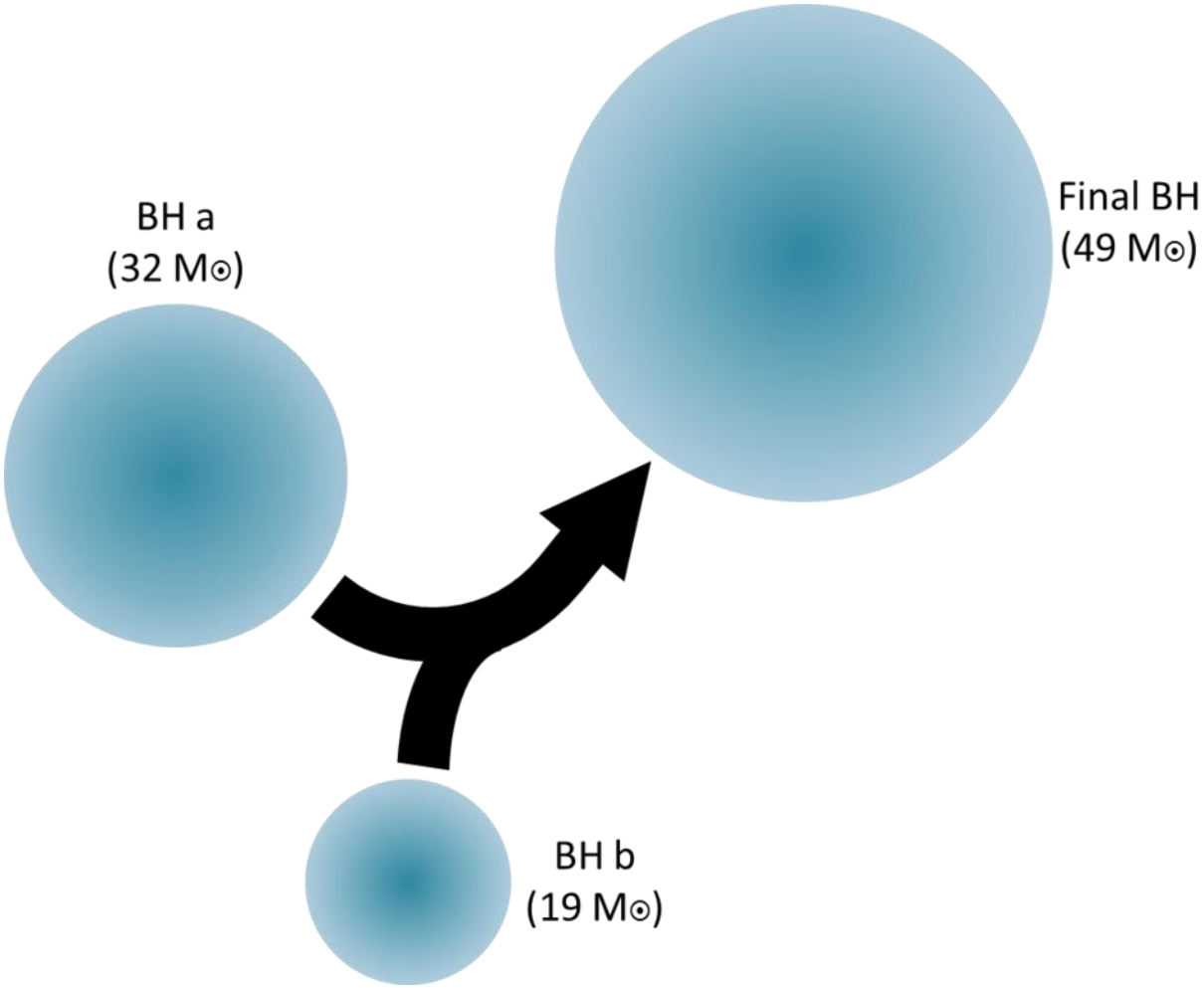
BH a
(32 M⊙)
Final BH
(49 M⊙)
BH b
(19 M⊙)

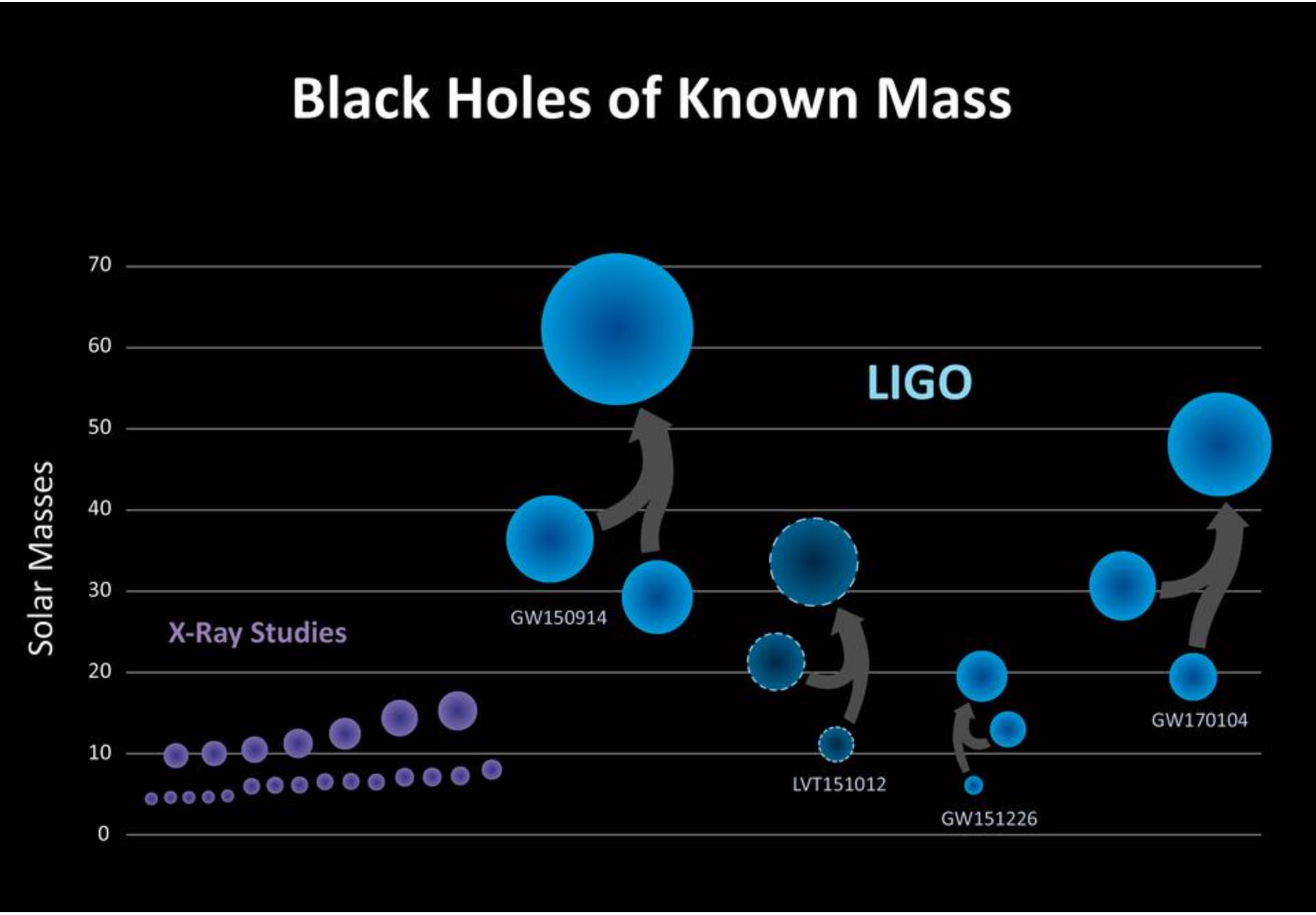
Black Holes of Known Mass
Solar Masses
70
60
50
40
30
20
10
0
LIGO
X-Ray Studies
GW150914
LVT151012
GW151226
GW170104

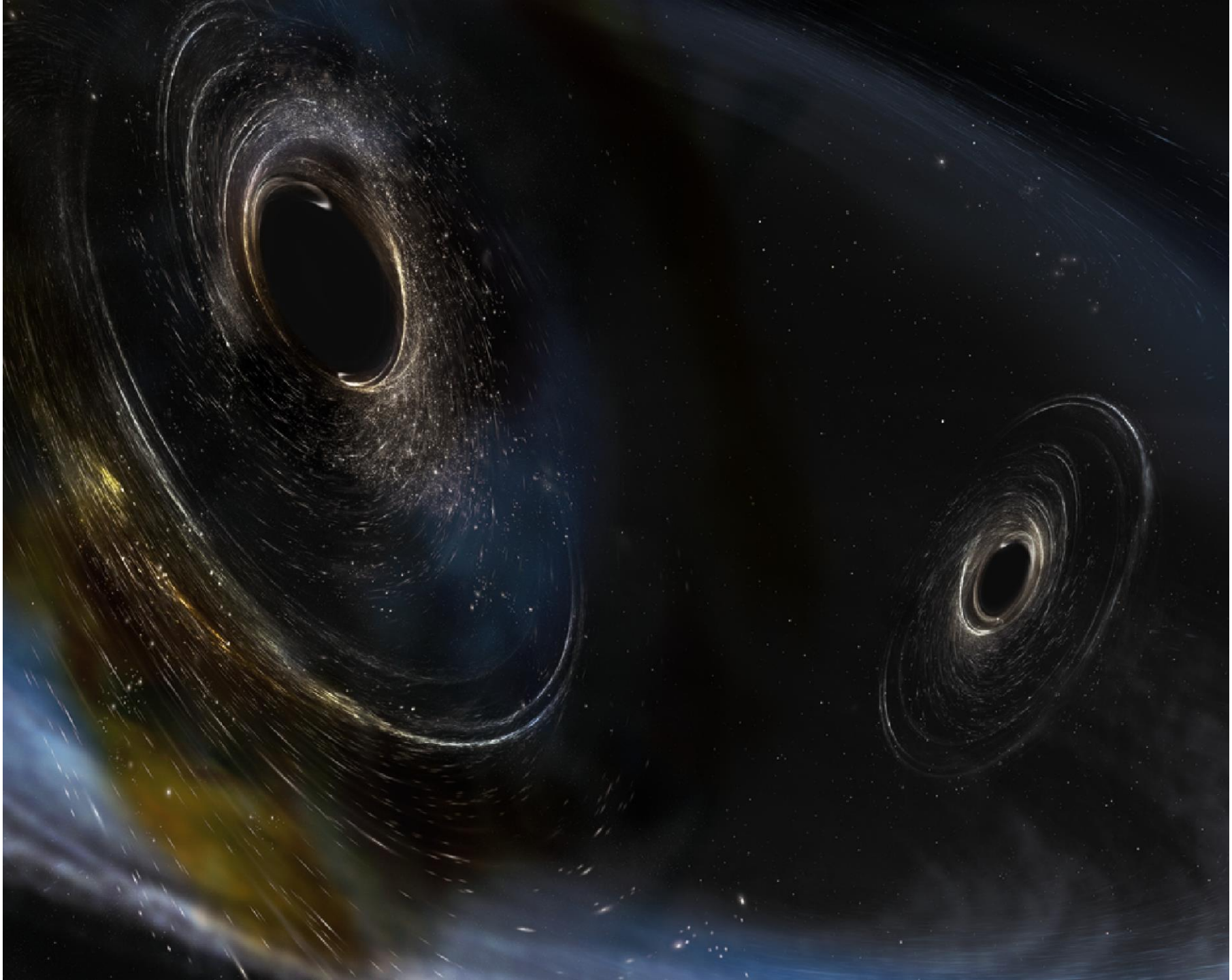

- On June 2, 2017 LIGO (Abbott et al. PRL 118, 21101 (2017)) reported about the discovery of the third GW event from merging the BHs with 31 and 19 solar masses at redshift z=0.19
- $m_g < 7.7 \times 10^{-23}$ eV

- **Conclusions**

- Constraints of graviton mass have been obtained
- The graviton mass constraints are found with other observational data
- Our constraints are consistent with LIGO’s ones
- The constraints could be improved with GRAVITY, E-ELT, TMT

- Thanks for your kind attention!
-

Constraints on graviton mass from S2 trajectory

- AFZ, D. Borka, P. Jovanovic, V. Borka Jovanovic gr-qc: 1605.00913v; JCAP (2016) :
- $\lambda_g > 2900$ AU $= 4.3 \times 10^{11}$ km with P=0.9 or
- $m_g < 2.9 \times 10^{-21}$ eV $= 5.17 \times 10^{-54}$ g